

PAPER • OPEN ACCESS

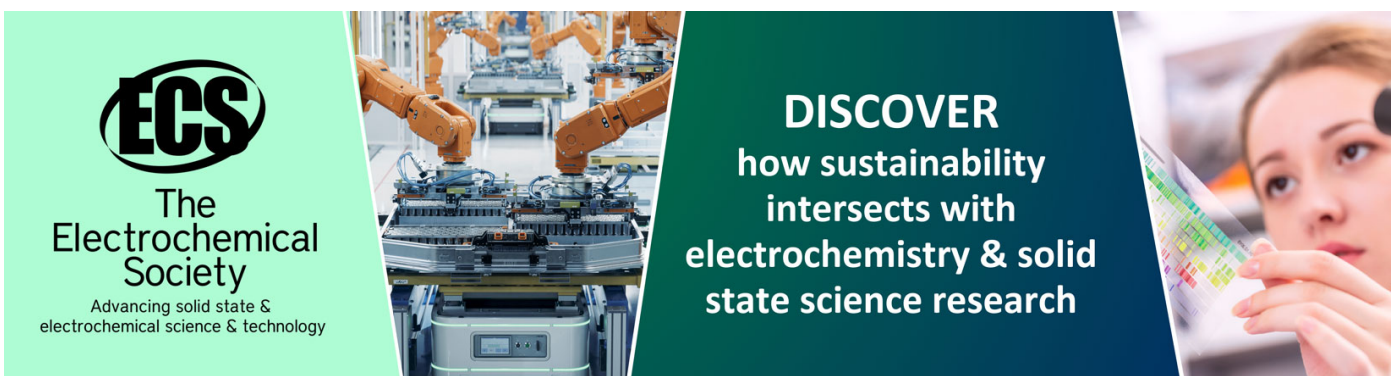
## Magnetic and structural Behavior of Fe-CoO Nanocomposites Mechanically Milled

To cite this article: Abderrahmane Younes *et al* 2019 *IOP Conf. Ser.: Mater. Sci. Eng.* **557** 012064

View the [article online](#) for updates and enhancements.

You may also like

- [Fabrication of nano ZrO<sub>2</sub> dispersed novel W<sub>73</sub>Ni<sub>16</sub>Ti<sub>6</sub>Nb<sub>5</sub> alloy by mechanical alloying and pressureless sintering](#)  
R. R. Sahoo, A. Patra and S. K. Karak
- [Effect of milling atmosphere on structural and magnetic properties of Ni-Zn ferrite nanocrystalline](#)  
Abdollah Hajalilou, Mansor Hashim, Reza Ebrahimi-Kahrizangi et al.
- [Fast and efficient approach to synthesis of ultra-fine TiC powder](#)  
Chang-Jiang Yang



**ECS**  
The  
Electrochemical  
Society  
Advancing solid state &  
electrochemical science & technology

**DISCOVER**  
how sustainability  
intersects with  
electrochemistry & solid  
state science research

# Magnetic and structural Behavior of Fe-CoO Nanocomposites Mechanically Milled

Abderrahmane YOUNES<sup>1,a,\*</sup>, Mohamed Khorchef<sup>1,b</sup>, Amirouche Bouamer<sup>1,c</sup> and Hichem Amar<sup>1,d</sup>

<sup>1</sup> Research Center in Industrial Technologies (CRTI) P.O.Box 64, Cheraga 16014 Algiers, Algeria

<sup>a</sup>younesabdo11@gmail.com, <sup>b</sup>m.khorchef@crti.dz, <sup>c</sup>a.bouamer@crti.dz, <sup>d</sup>h.amar@crti.dz

**Abstract.** The Fe<sub>60</sub>(CoO)<sub>40</sub> nanostructured alloys have been prepared from pure iron and cobalt oxide powders by mechanical alloying technique within a high energy planetary ball-mill. Morphology, microstructural and magnetic properties of this powder were investigated by a Scanning Electron Microscope (SEM), X-ray diffraction (XRD) and Vibrating sample magnetometer (VSM). The effect of time of milling on magnetic behaviour of Fe(CoO) nanostructured composite has been investigated. Apparition of new phase polycrystalline sample having a size in the range of 12 and 26 nm, it is confirmed by X-ray diffraction testing. The enhanced magnetic properties and structural behaviour of the nanoparticle are due by the diminution of size of crystallite. After 40 hours of milling, the appearance of spinel structure of CoFe<sub>2</sub>O<sub>4</sub>. The reduction in particle size leads to a significant increase in magnetic hardening, the coercive field at room temperature increases from 6 Oe to 208 Oe

## 1. Introduction

A magnetic powder material is among the first areas of research in recent time for material researchers in accordance to its emerging potential applications in various technological fields and as well as new structural and magnetic properties at the essential level [1]. The CoO is used extensively in the ceramics industry and transition metal oxides, the CoO have higher magneto-crystalline anisotropy [2-3]. In other way, iron nanostructured particles have attracted significant attention for the reason of their attractive magnetic properties and applications in high density magnetic recording media [4]. The main applications of cobalt iron oxide nanoparticles are as a nanoscale magnetic material with applications in molecular imaging and drug delivery [5-6]. In this paper, we are studying the magnetic properties in the Fe/CoO nanostructured alloy. The effect of crystallite size in the hysteresis loops has been observed by vibrating sample magnetometer.

## 2. Experimental procedure

The particle size and purity of elemental powders are 80 μm, 99.5% for Fe and 100 μm, 99.9% for CoO. The mixture of Fe, CoO powders was grinded in planetary ball mill (PM400) under controlled atmosphere used a hard chromium grinding balls. The initial powder mixtures are contains of 60% wt of Fe and 40% wt of (CoO). The mass ratio of powder to balls was approximately 1:30. The time of milling was varied from 5 to 40 hours. The mechanical alloying method was used to elaborate Fe<sub>60</sub>(CoO)<sub>40</sub> powder alloys and to decrease the particles sizes after severe plastic deformation.

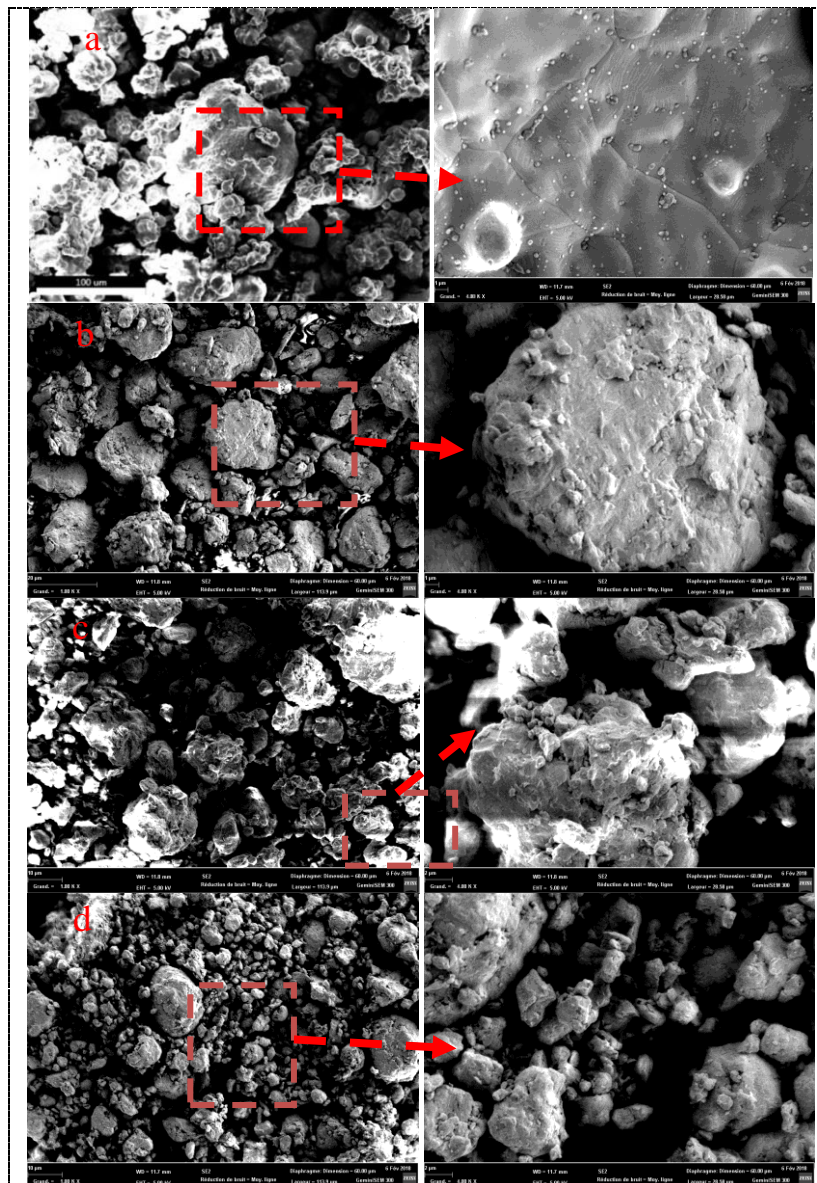


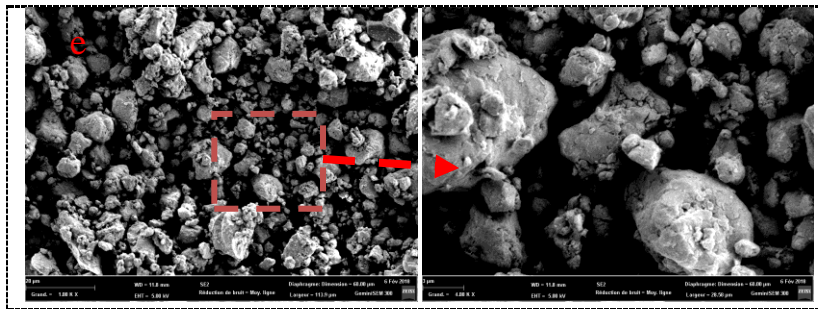
Morphology, particle size and particle distribution of powders alloy formed after mechanical milling was characterized by scanning electron microscopy (Gemini SEM 300) attached with Energy Dispersive X-ray unit (EDX). Crystallite size, lattice strain and lattice parameters were determined by X-ray diffraction analysis (XPERT PRO) using Co  $K\alpha$  radiation. Magnetic measurement properties were determined by Vibrating Sample Magnetometer (VSM).

### 3. Results and Discussion

#### 3.1. Powder morphology

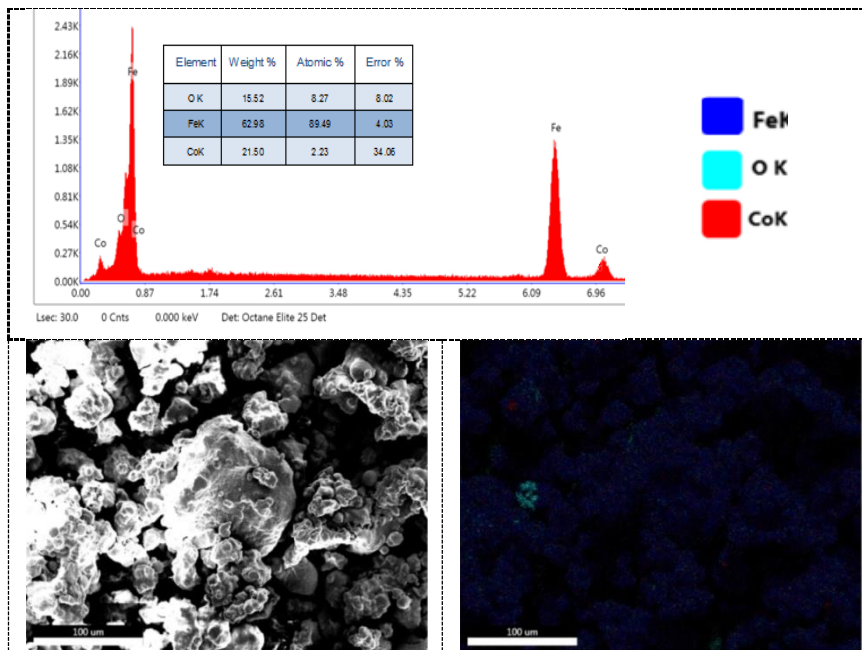
Morphology of the  $\text{Fe}_{60}(\text{CoO})_{40}$  powder mixture milled for different times was shown in figure 1. During the milling time,  $\text{Fe}_{60}(\text{CoO})_{40}$  powder having uniform particle size distribution, flattened and irregular shapes, this morphology is caused by severe plastic deformation, welding process and fracture process [12-13]. Cold welding and fracture process lead to considerable changes in the morphology of the powder particles during mechanical alloying. The mean particle size of  $\text{Fe}_{60}(\text{CoO})_{40}$  powder alloy after 40 hours of milling (figure 1.e) is smaller than 5, 10,15 and 25 hours of milling, indicating that the milling effect speed up the reduction of particle size.





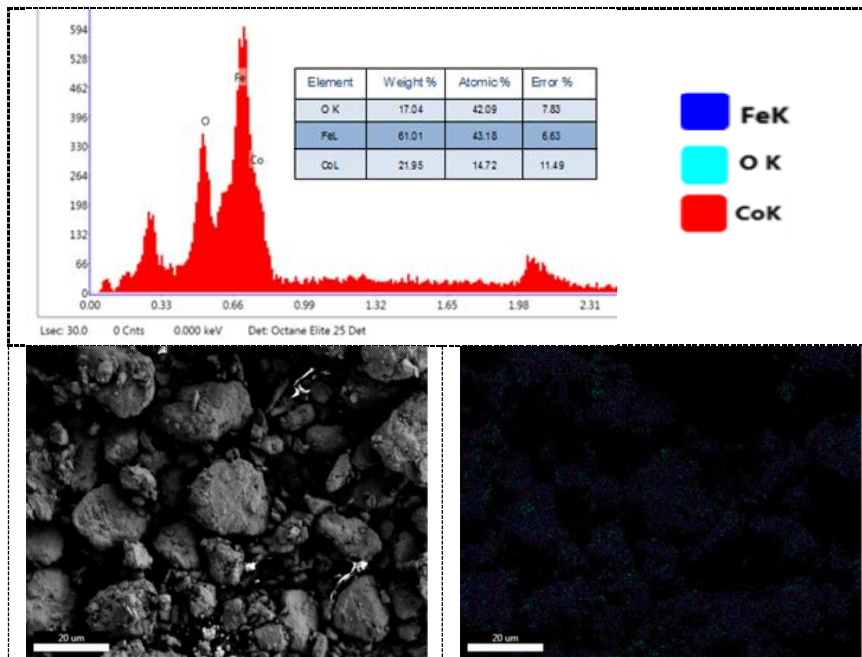
**Figure 1.** Micrographie by SEM of the  $\text{Fe}_{60}(\text{CoO})_{40}$  powder alloy for different milling time: a(5 h), b(10 h), c(15 h), e(25 h) and d(40h).

Figure 2 show the repartition of chemical elements determined using Energy Differential Scanning, the EDS analysis; indicate the existence and the same percentage of chemical elements in the  $\text{FeCoO}$ . We have found a relationship between the composition of initial powder and the milling powder studied in this work. The spectrum of existence element of  $\text{FeCoO}$  alloy powder shows the presence of different element Fe, Co and O.



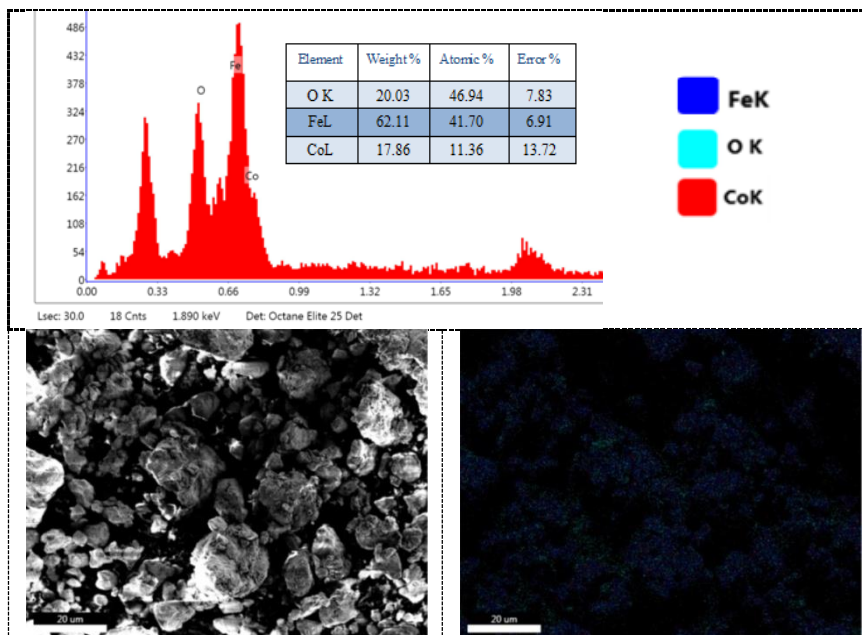
**Figure 2.a.** EDS spectrum and distribution of different elements of the  $\text{Fe}_{60}(\text{CoO})_{40}$  powder alloy milled to 5h

The repartition of different elements Fe, Co and O are homogeneously distributed on  $\text{Fe}_{60}(\text{CoO})_{40}$  alloy powder, this distribution are caused by mechanical milling parameters, concerning the value of mass percentages of Fe, CoO determined by EDS analysis are 62.98 %wt, 37.02%wt respectively (figure 2a).



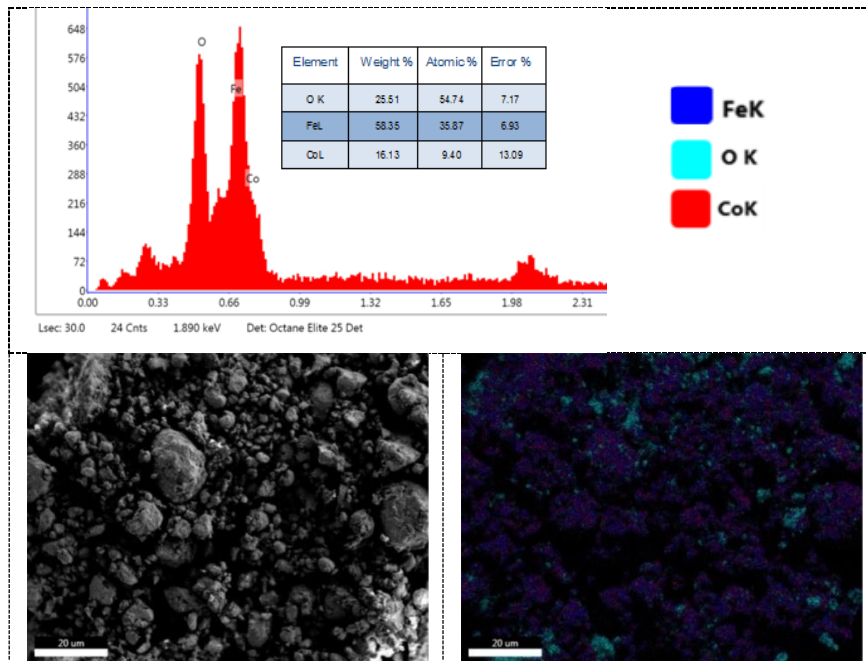
**Figure 2b.** EDS spectrum and distribution of different elements of the  $\text{Fe}_{60}(\text{CoO})_{40}$  powder alloy milled to 10h

Figure 2b shows the uniformly distributed of Fe, Co and O in the  $\text{Fe}_{60}(\text{CoO})_{40}$  powder milled to 10h, and the mass percentage of Fe and CoO is 61.01 % Wt and 38.99%Wt respectively determined by EDS analysis.



**Figure 2c.** EDS spectrum and distribution of different elements of the  $\text{Fe}_{60}(\text{CoO})_{40}$  powder alloy milled to 15h.

The cartography of different element presented in figure 2c shows that the repartition of Fe, Co and O are homogeneous and the mass percentage of Fe and CoO is 62.11 % wt and 37.89%wt respectively determined by EDS analysis



**Figure 2d.** EDS spectrum and distribution of different elements of the  $Fe_{60}(CoO)_{40}$  powder alloy milled to 15h.

The distribution of Fe, Co and O in the  $Fe_{60}(CoO)_{40}$  milled to 25 hours presented in figure 2d shows that have a homogeneity of this elements in  $Fe_{60}(CoO)_{40}$  powder milled to 25h, and the mass percentage of Fe and CoO is 58.35 % wt and 41.65%wt respectively determined by EDS analysis.

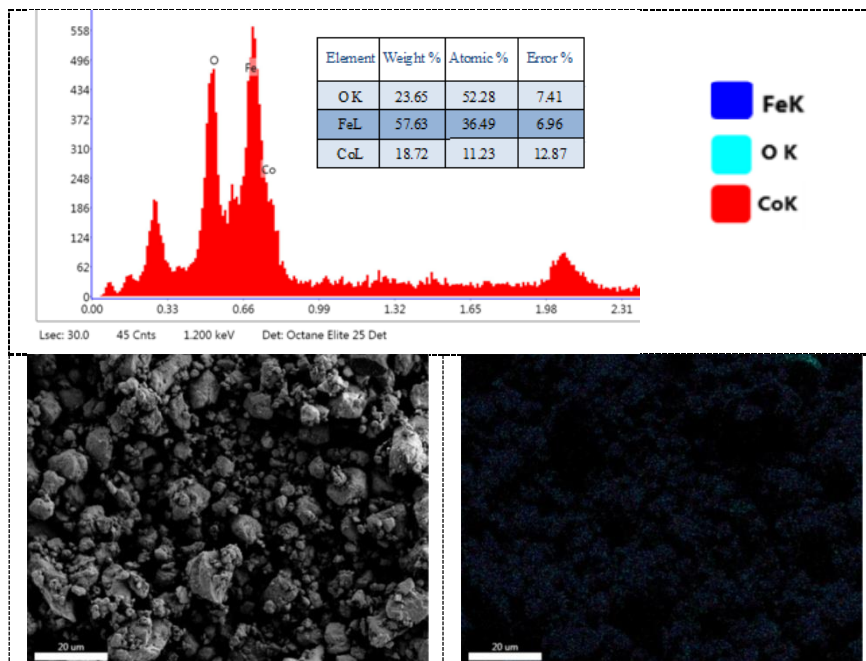


**Figure 2e.** EDS spectrum and distribution of different elements of the  $Fe_{60}(CoO)_{40}$  powder alloy milled to 40h.

The EDS analysis presented in figure 2e shows the presence of Fe and CoO in  $\text{Fe}_{60}(\text{CoO})_{40}$  powder milled to 40h with mass percentage 57.63 % Wt and 42.37% Wt respectively. The repartition of these elements (Fe, Co and O) presented in figure 2d shows a good homogeneity in the powder alloy.

### 3.2. Structural characterization of $\text{Fe}_{60}(\text{CoO})_{40}$

Figure 3 shows the progression of the crystallites size and lattice strain, kinetics of formation, evolution of lattice parameters determined by X-ray diffraction analysis of  $\text{Fe}_{60}(\text{CoO})_{40}$  powder alloy during mechanical milling time to 5 until 40hours.

Figure 3 has shown the presence of Fe, CoO and  $\text{CoFe}_2\text{O}_4$  after milling time, the corresponding peaks in iron decrease in intensity. In parallel, the displacement of peaks of iron for a new position of Bragg angle is caused by the phenomenon of formation of alloy. After 40 hours of milling appeared a new peak of  $\text{CoFe}_2\text{O}_4$ .

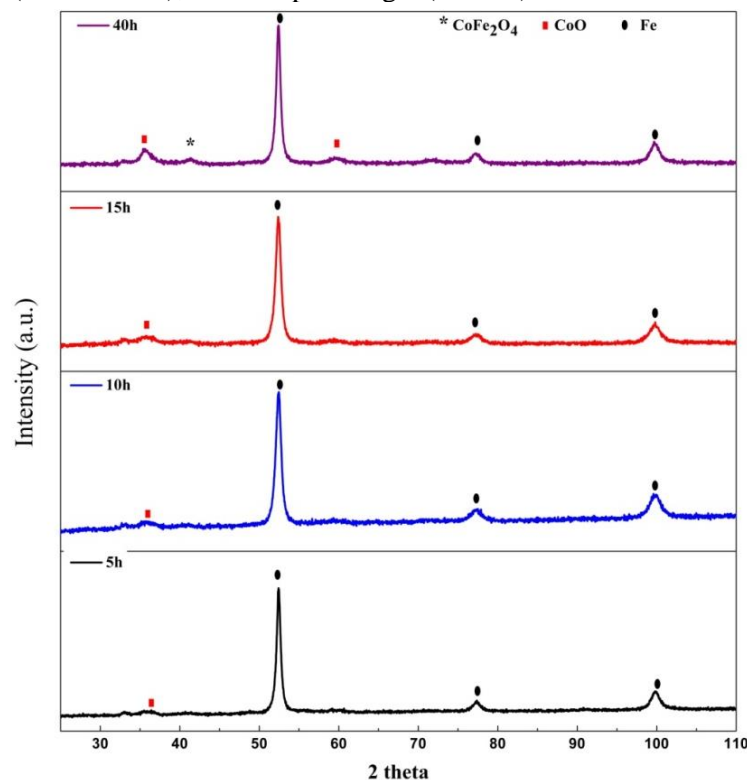
X-Ray diffraction measurements are used to determine the lattice parameter of the different phases presented in  $\text{Fe}_{60}(\text{CoO})_{40}$  powder alloy in function of milling time, the principle (hkl) plane (110) were used to determined the lattice parameter according to equation (Eq. 1) [14]:

$$\frac{1}{d^2} = \frac{h^2 + k^2 + l^2}{a^2} \quad (1)$$

The crystallite size (D) was calculated from the width at half maximum (FWHM) using Scherer equation according to equation (Eq. 2)

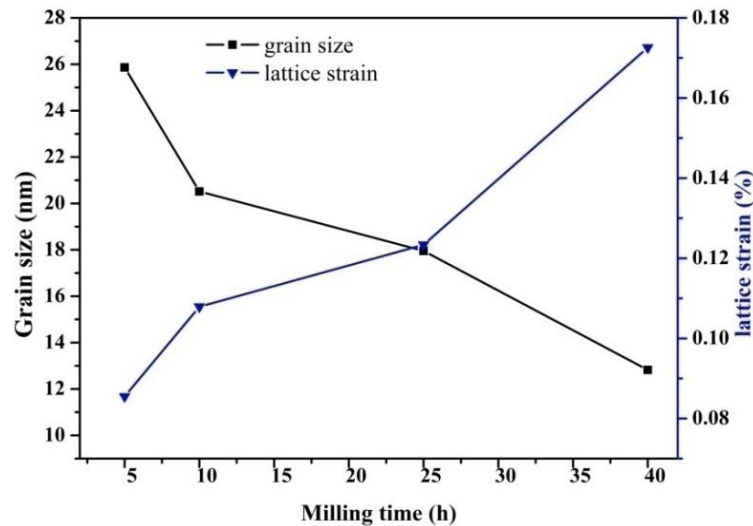
$$D = \frac{0.9 * \lambda}{FWHM * \tan \theta} \quad (2)$$

Where  $\lambda = 1.78901$  (Co radiation),  $\theta$  is the peak angle (radians).



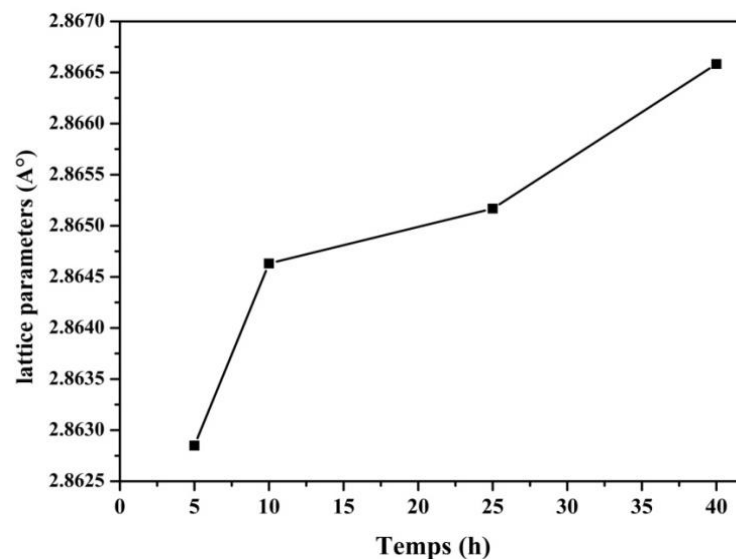
**Figure 3** X-ray diffraction of  $\text{Fe}_{60}(\text{CoO})_{40}$  powder mixture milled for different time of mechanical milling.

Figure 4 shows the variation of average crystallite size and lattice strain of  $\text{Fe}_{60}(\text{CoO})_{40}$  powder alloy during mechanical milling time, the reduction of the size of crystallite is due of the increase of energy stocked inside particles during plastic deformation. The increase of lattice strain and the decrease of the size of crystallite in function of mechanical milling time are caused by distortion effect in the crystallite lattice with a high density of dislocations.



**Figure 4.** Change of average crystallite size and lattice strain of  $\text{Fe}_{60}(\text{CoO})_{40}$  powder alloy during mechanical milling time.

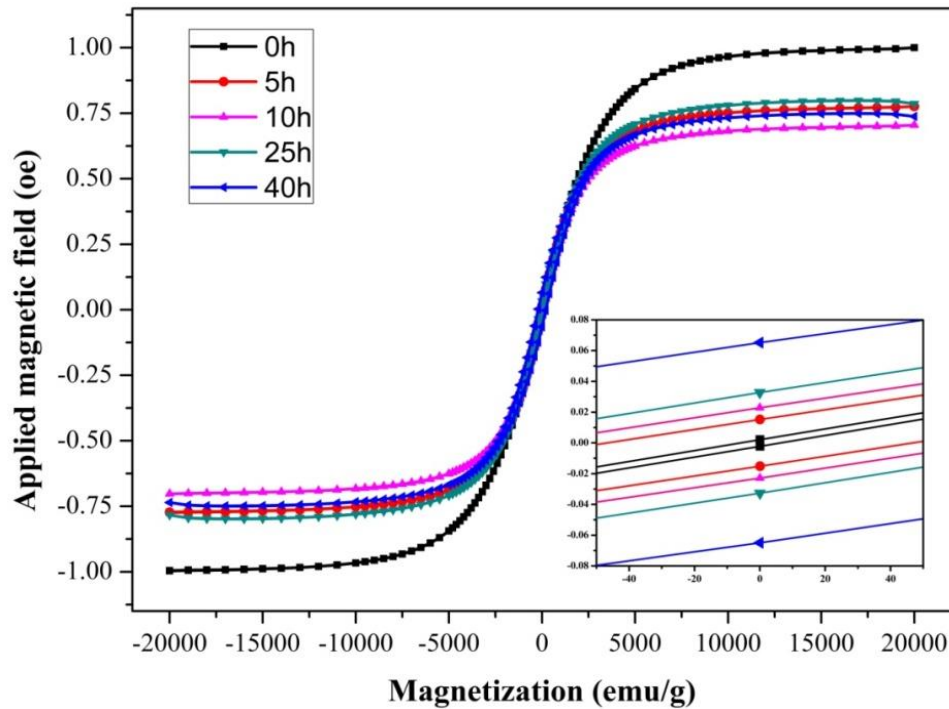
Figure 5 shows the Change of the lattice parameter of  $\text{Fe}_{60}(\text{CoO})_{40}$  powder alloy during of mechanical milling time, the increase in the lattice parameter during milling time has been noticed. This variation is easily explained in the first step by the dislocation introduced during mechanical alloying. The decrease in the next step can be explained by a dynamic equilibrium between the mechanical alloying effects and the restoration of particle powder.



**Figure 5.** Change of the lattice parameter of  $\text{Fe}_{60}(\text{CoO})_{40}$  powder alloy during of mechanical milling time.

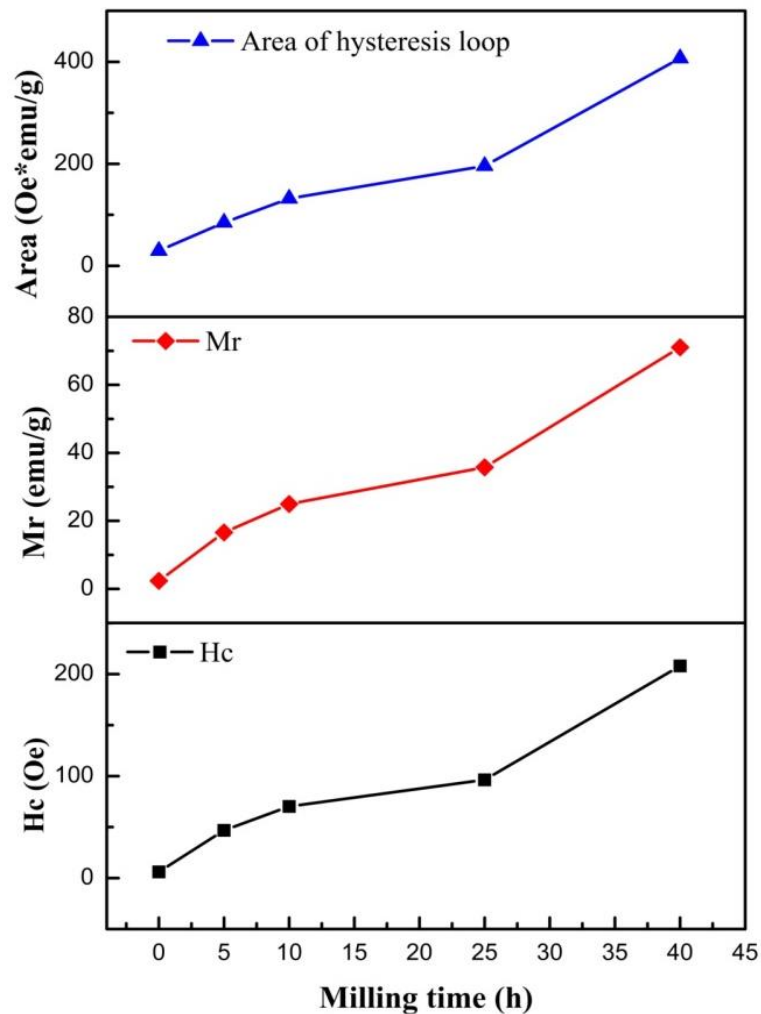
### 3.3. Magnetic measurements

Figure 6 show the hysteresis loops for  $\text{Fe}_{60}(\text{CoO})_{40}$  powder alloy milled during mechanical alloying. The hysteresis loops determined seem as soft magnetic materials with the magnetic properties varied versus mechanical milling time. The variation of coercive force ( $H_c$ ), magnetization saturation ( $M_s$ ), and residual magnetization ( $M_r$ ) during mechanical alloying is shown in figure 6.



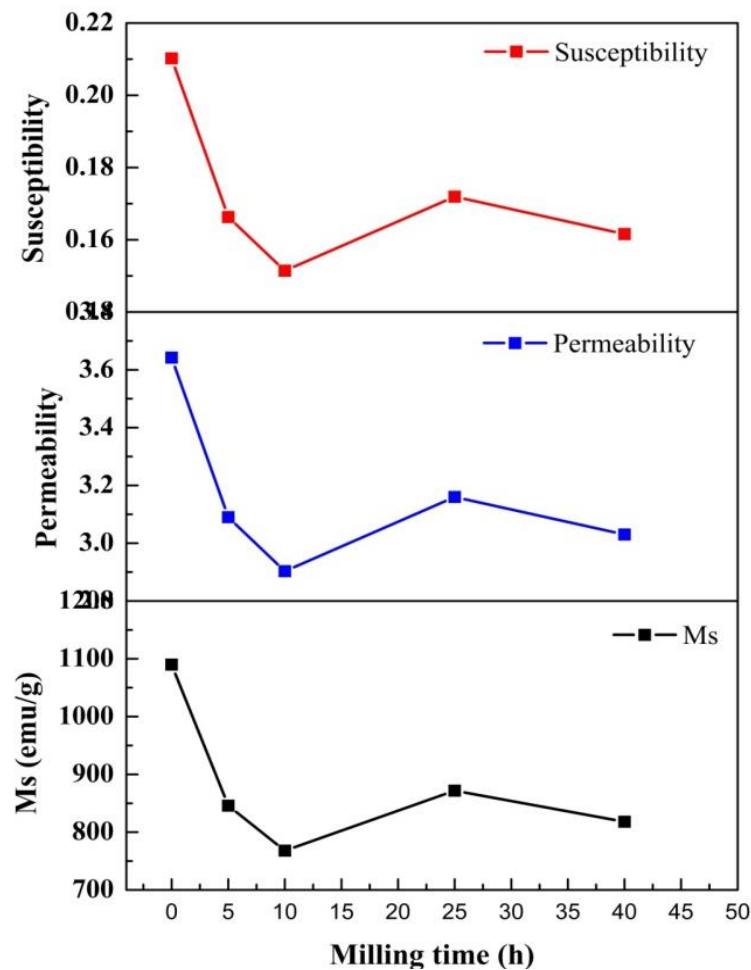
**Figure 6.** Hysteresis curve of  $\text{Fe}_{60}(\text{CoO})_{40}$  powders alloy for different milling time.

Figure 7 shows the variation of coercivity, remanence and area of hysteresis loops in function of milling time of  $\text{Fe}_{60}(\text{CoO})_{40}$  powder alloy. These variation of coercivity, remanence and area of hysteresis loop have the same evolution, we can explain this rise by many factors such as reduction of crystallite size, internal stress, dislocation density and impurities which are introduced during the mechanical alloying process (figure .7).



**Figure 7.** Evolution of area of hysteresis loop, Mr and Hc of  $\text{Fe}_{60}(\text{CoO})_{40}$  powder alloy for different milling time.

Figure 8 shows the evolution of susceptibility, permeability and Ms of  $\text{Fe}_{60}(\text{CoO})_{40}$  powder alloy for different milling time, The variations of saturation magnetization, susceptibility and permeability during milling time of the powder alloy are shown in figure 8. The reductions of particle size decrease the magnetocrystalline anisotropy; this reduction is due to the magnetic effect of nanoparticles that are oriented in an arbitrary manner, these parameters are highly dependent on the chemical composition of  $\text{Fe}_{60}(\text{CoO})_{40}$  powder alloy



**Figure 8.** Evolution of susceptibility, permeability and Ms of  $\text{Fe}_{60}(\text{CoO})_{40}$  powder alloy for different milling time

#### 4. Conclusion

The  $\text{Fe}_{60}(\text{CoO})_{40}$  alloy powders were successfully elaborated by mechanical milling technique using PM400. The magnetic behavior, morphological of powder and structural parameters of  $\text{Fe}_{60}(\text{CoO})_{40}$  powder alloy could be determined. The structural parameters such as the crystallite size modify the magnetic behavior of  $\text{Fe}_{60}(\text{CoO})_{40}$  powder alloy.

The mappings of the powders alloy are distributed in a homogeneous way and kept the same proportion with the initial chemical composition. The coercivity of the  $\text{Fe}_{60}(\text{CoO})_{40}$  alloy highly depends on the structural parameters, the saturation magnetization is highly dependent on the chemical composition of powder alloy.

#### Reference

- [1] S.D. Bader, Colloquium: opportunities in nanomagnetism, *Reviews of Modern Physics* 78:1, (2006)
- [2] N.R. Panda, S.P. Pati, A. Das, D. Das, Annealing temperature induced phase evolution and exchange bias properties of Fe/CoO nanocomposites, *App. Surf. Sc.* 449 (2018) 654-659.
- [3] A. J. Sievers, III, and M. Tinkham, Far Infrared Antiferromagnetic Resonance in MnO and NiO *Phys. Rev.* 129 (1963) 1566-1571.
- [4] J.L. Dormann, , D. Fiorani, *Magnetic properties of fine particles*, North-Holland delta series, Amsterdam, (1992) 323

- [5] J. Kudr, , Y. Haddad, , L. Richtera, , Z. Heger, , M. Cernak, , V. Adam, and O. Zitka, , Magnetic Nanoparticles: From Design and Synthesis to Real World Applications, *Nanomaterials*, 7(9) (2017) 243.
- [6] S. P. Pati, D. Das, Inter-particle and collective states of interactions in mechanically milled Fe(CoO) nanocomposites, *J. Nanopart. Res.* 16:2278 (2014) 1-12.
- [7] G. C. Lavorato, E. Lima Jr, D. Tobia, D. Fiorani, H. E. Troiani, R.D. Zysler, E.L.Winkler, Size effects in bimagnetic CoO/CoFe<sub>2</sub>O<sub>4</sub> core/shell nanoparticles, *Nanotechnology* 25:355704 (2014) 1-9
- [8] S. P. Pati, A. Roychowdhury, S. Kumar, and D. Das, Signature of exchange bias and spin-glass like phenomena in Fe/CoO nanocomposite, *Journal of applied physics* 113 (2013) 17D708(1)-17D708(3).
- [9] R. Abrudan, J. Miguel, M. Bernien, C. Tieg, M. Piantek, J. Kirschner, and W. Kuch, Structural and magnetic properties of epitaxial Fe/CoO bilayers on Ag(001), *Physical review B* 77 (2008) 014411(1)- 014411(7).
- [10] E. Młynczak, , B. Matlak, , A. Kozió-Rachwa, , N. Gurgu, Spiridis, and J. Korecki, Fe/CoO(001) and Fe/CoO(111) bilayers: Effect of crystal orientation on the exchange bias, *Physical Review B* 88 (2013) 085442(1)- 085442(10).
- [11] S.R. Mishra, I. Dubenko, J. Losby, S. Roy, N. Ali, and K. Marasinghe, Magnetic Behavior of Mechanically Milled FeNi-CoO Nanocomposites, *IEEE Transactions on magnetics*, 40(4) , (2004) 2716 - 2720.
- [12] A. Younes, N. E. Bacha, M. Zergoug, N. Dilmi, Structural and magnetic properties of Fe–Co/Al<sub>2</sub>O<sub>3</sub> nanocomposite powder produced by mechanical alloying, *Powder Metallurgy and Metal Ceramics*, 56 (3) (2017)148-157.
- [13] A. Younes, N.E. Bacha, M. Zergoug, M. Gousmine, H. Dehdouh, and A. Bouamer, Effect of Grain Size of Nano Composite on Raman and Magnetic Proprieties, *Applied Mechanics, Behavior of Materials, and Engineering Systems* , 32(1) (2017) 425-433.
- [14] A. Younes, N. Dilmi, M. Khorchef, A. Bouamer, N-E. Bacha, and M. Zergoug, Structural and magnetic properties of FeCuNi nanostructured produced by mechanical alloying, *Applied Surface Science* 446 (2018) 258–265.